Supplementary Information

Facial route for high mass loading amorphous NiCo-MOF as high-performance electrode materials toward asymmetric supercapacitor

Junnan Yao[a], Yajun Ji*[a], Faxue Lu[a], Dong Shi[a], Lijun Pei[a]

[a] *School of Materials and Chemistry, University of Shanghai for Science and Technology, Jungong Road 334#, 200093 Shanghai, China.* *Corresponding author: E-mail: jiyajun@usst.edu.cn
Fax: +86 21 65667144; Tel: +86 21 65667144

Experimental section

Materials

$Ni(NO_3)_2·6H_2O$, $Co(NO_3)_2·6H_2O$, m-phthalic acid, EtOH and KOH were purchased from Sinopharm Chemical Reagent Co., Ltd. The active carbon (AC) was provided by Nanjing XFNANO Materials Tech Co., Ltd. The nickel foam (NF) substrate was cut to 2 cm × 1 cm and carefully cleaned by ultrasonication in deionized water and absolute ethanol subsequently.

Synthesis of NiCo-MOF

At first, 0.166 g of m-phthalic acid, 0.193 g of $Ni(NO_3)_2·6H_2O$ and 0.096g $Co(NO_3)_2·6H_2O$ were dissolved in 5 mL H_2O and 15 mL EtOH with stirring at room temperature. Then, the above solution and one piece treated NF was transferred to a 50 mL Teflon-lined stainless-steel autoclave and heated at 150 °C for 12 h. After the autoclave was cooled to room temperature, the resulting product was washed with deionized water and ethanol three times separately and dried for 12 h at 60 °C. The obtained material was named as NiCo-MOF. And the average mass loading of NiCo-MOF was about 10.3 mg cm^{-2} after calculating the mass of nickel foam before and after reaction.

Characterization

The crystal structure of the sample was characterized by XRD (BRUKER D8 ADVANCE). XPS (Kratos XSAM 800) was used to study the oxidation states of various elements in the sample. The surface morphology and microstructure of the sample was studied by SEM (ZeissSupra 55) and HRTEM (JEOL 2100F).

Electrochemical measurements

Electrochemical measurements were carried out in a standard three-electrode system with 1 M KOH as electrolyte. The synthesized sample was used as the working electrode, platinum wire as the counter electrode and standard Ag/AgCl electrode as the reference electrode. The electrochemical performance of the synthesized sample was measured on CHI 660E (Chenhua) electrochemical workstation, including cyclic voltammetry (CV), constant current charge-discharge (GCD) and electrochemical impedance spectroscopy (EIS). According to the GCD curve, the areal capacitance of the product was calculated based on the following equation (1):

$$C_a = \frac{I \times t}{S \times \Delta V} \quad (1)$$

where C_a (F cm^{-2}) is the areal capacitance, I (A) is the discharge current, t (s) is the discharge time, S (cm^2) is the geometrical area of the electrode and ΔV is the potential window.

In 1 M KOH electrolyte solution, with NiCo-MOF as the positive electrode and active carbon (AC) as the negative electrode, the asymmetric device was packaged as an example of practical application. In order to obtain the optimized supercapacitor, the mass of cathode and anode materials was calculated according to the following equation (2) to maximize the energy density of the device.

$$\frac{m_+}{m_-}=\frac{C_-\times\Delta V_-}{C_+\times\Delta V_+} \tag{2}$$

where m_+ and m_- are the mass of NiCo-MOF and AC on the NF separately, C_- and C_+ are the areal capacitance of the positive and negative electrodes respectively, and ΔV_- and ΔV_+ are the potential window of the positive and negative electrodes, respectively.

The corresponding energy density (mWh cm^{-2}) and power density (mW cm^{-2}) of the ASC device could be calculated from the following equations (3) and (4):

$$\mathrm{E}=\frac{1}{2}CV^2 \tag{3}$$

$$P=\frac{E}{\Delta t} \tag{4}$$

where C (F cm^{-2}) is the specific capacitance of the ASC calculated from the GCD curve, V (V) is the potential window of the ASC, and Δt (S) is the discharge time of the ASC obtained from the GCD curve.

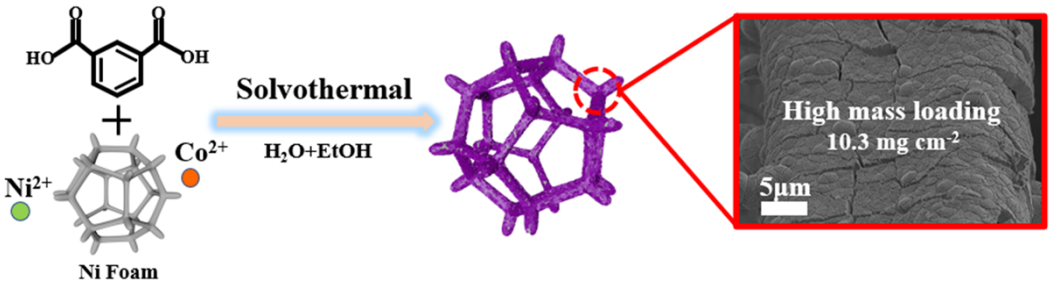

Fig. S1 Schematic illustration of the synthesis of NiCo-MOF.

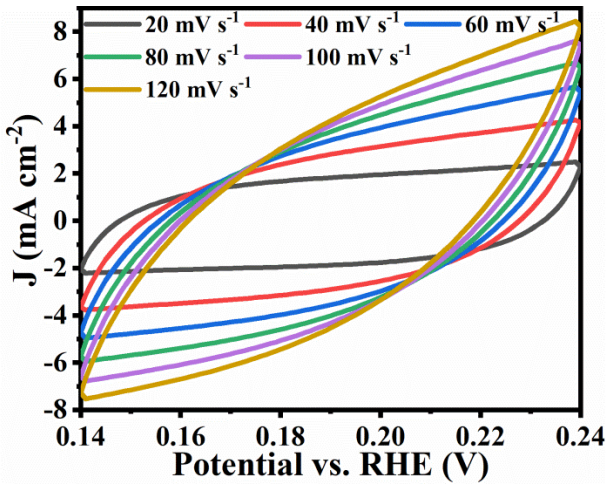

Fig. S2 CV curves of NiCo-MOF at different sweep speeds in the potential range of 0.14-0.24 V.

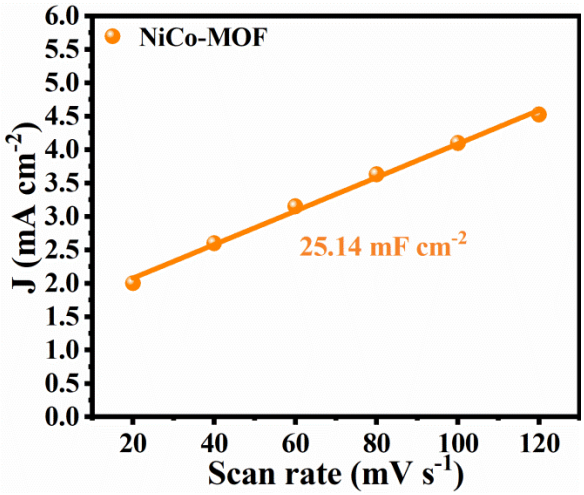

Fig. S3 Current density at different scan rates in the window of 0.14–0.24 V vs. Ag/AgCl for NiCo-MOF after the electrochemical activation.

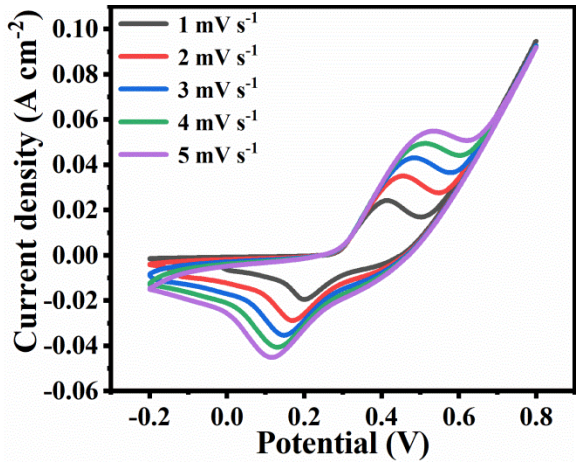

Fig. S4 CV curve of NiCo-MOF with the scan rate range from 1 mV s^{-1} to 5 mV s^{-1} in the potential range of -0.2-0.8 V.

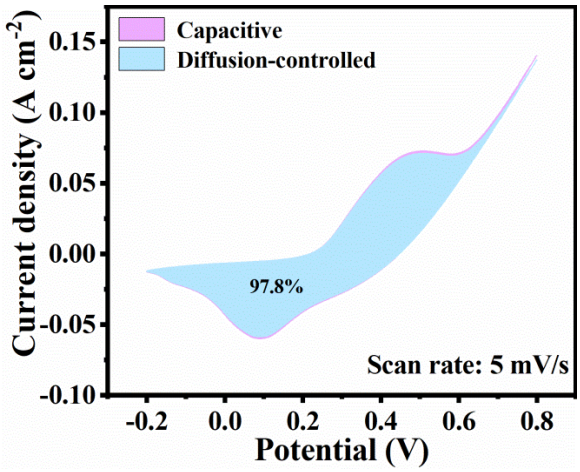

Fig. S5 Separation of the diffusion-controlled capacitive and capacitive currents of the NiCo-MOF at a scan rate of 5 mV s^{-1}.

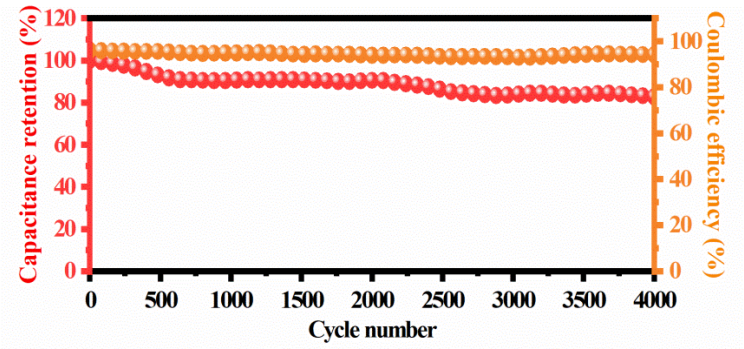

Fig. S6 Cycling performance and Coulomb efficiency of NiCo-MOF at 20 mA cm^{-2}.

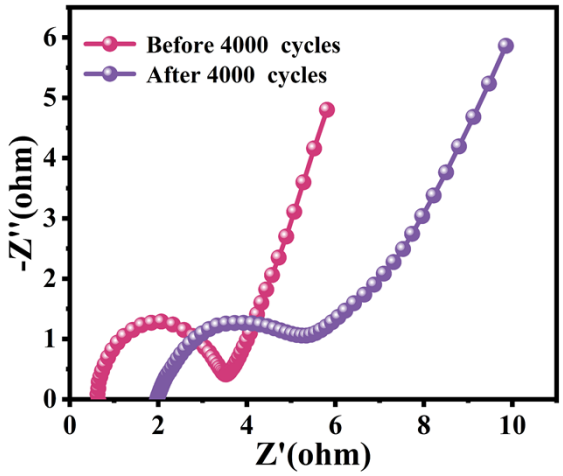

Fig. S7 EIS curves of NiCo-MOF before and after the stability test.

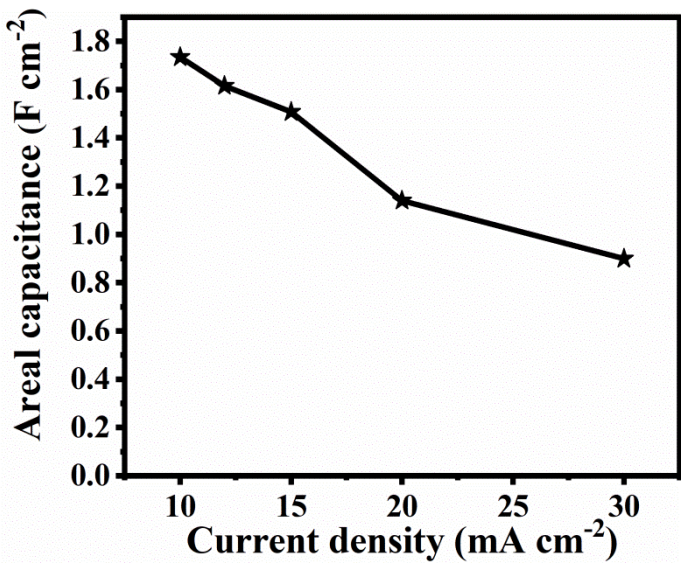

Fig. S8 The areal capacitance of ASC at different current densities.

Table.S1 Comparison of the electrochemical performance based on NiCo-MOF in this work with other materials.

Electrode Materials	Minimum current density (mA cm^{-2})	Specific capacitance (F cm^{-2})	Maximum current density (mA cm^{-2})	Specific capacitance (F cm^{-2})	Ref.
NiCo-MOF	5	9.72	20	7.15	**This work**
NCM/rGO-200	1	4.31	30	1.56	[s1]
PCN-224@PEDOT/PMo12–CC-I	5	4.08	20	3.38	[s2]
NiCo-OHs	2	9.00	50	4.50	[s3]
$NiCo_2O_4$/graphene	2	3.84	50	2.75	[s4]
$Cu(OH)_2/Co_2(OH)_2CO_3$	2	1.31	50	0.74	[s5]
Co/Mn-MOF	3	2.76	20	1.73	[s6]
NiCo-MOF	1	5.84	10	4.56	[s7]
NiCo-BDC-MOF NS/NF	2	8.80	50	3.61	[s8]
NF-NiO-2	1	2.08	50	1.21	[s9]
Ni-decorated Co_9S_8	1	5.64	20	5.01	[s10]

References

[s1] C. Shi, H. Cao, S. Li, L. Guo, Y. Wang and J. Yang, J Energy Storage, 2022, **54**,105270.

[s2] B. Wang, S. Liu, L. Liu, W.-W. Song, Y. Zhang, S.-M. Wang and Z.-B. Han, J. Mater. Chem. A, 2021, **9**, 2948-2958.

[s3] W. Hu, H. Fu, L. Chen, X. Wu, B. Geng, Y. Huang, Y. Xu, M. Du, G. Shan, Y. Song, Z. Wu and Q. Zheng, Chem. Eng. J, 2023, **451**,138613.
[s4] H. Feng, S. Gao, J. Shi, L. Zhang, Z. Peng and S. Cao, Electrochim. Acta, 2019, **299**, 116-124.
[s5] H. Liu, Z. Guo, X. Xun and J. Lian, J. Mater. Sci, 2019, **30**, 11952-11963.
[s6] Y. Seo, P. A. Shinde, S. Park and S. Chan Jun, Electrochim. Acta, 2020, **335**,135327.
[s7] S. Huang, X.-R. Shi, C. Sun, X. Zhang, M. Huang, R. Liu, H. Wang and S. Xu, Appl. Surf. Sci, 2022, **572**,151344.
[s8] Y. Ling, Y. Wang, W. Zhao, J. Zhou, K. Chen, K. Tao and L. Han, Inorg Chem, 2022, **61**, 3832-3842.
[s9] S. Zhou, S. Wang, S. Zhou, H. Xu, J. Zhao, J. Wang and Y. Li, Nanoscale, 2020, **12**, 8934-8941.
[s10] Y. Wen, Y. Liu, S. Dang, S. Tian, H. Li, Z. Wang, D. He, Z.-S. Wu, G. Cao and S. Peng, J. Power Sources, 2019, **423**, 106-114.